A Letters Journal Exploring the Frontiers of Physics

February 2008

EPL, **81** (2008) 34002
doi: 10.1209/0295-5075/81/34002

www.epljournal.org

Laser Doppler measurement of inertial particle and bubble accelerations in turbulence

R. Volk[1], N. Mordant[2], G. Verhille[1] and J.-F. Pinton[1]

[1] *Laboratoire de Physique de l'École normale supérieure de Lyon, CNRS UMR5672 46 Allée d'Italie, 69007 Lyon, France*
[2] *Laboratoire de Physique Statistique de l'École normale supérieure de Paris, CNRS UMR8550 24 rue Lhomond, 75005 Paris, France*

received 10 October 2007; accepted in final form 26 November 2007
published online 31 December 2007

PACS 47.27.Jv – High-Reynolds-number turbulence
PACS 47.27.Gs – Isotropic turbulence; homogeneous turbulence
PACS 47.80.-v – Instrumentation and measurement methods in fluid dynamics

Abstract – We use an extended laser Doppler technique to track optically the velocity of individual particles in a high Reynolds number turbulent flow. The particle sizes are of the order of the Kolmogorov scale and the time resolution, 30 microseconds, resolves the fastest scales of the fluid motion. Particles are tracked for mean durations of the order of 10 Kolmogorov time scales and their accelerations are measured. For neutrally buoyant particles (fluid tracers), this technique matches the performance of the silicon strip detector technique introduced at Cornell University (Voth G. A. *et al.*, *J. Fluid Mech.*, **469** (2002) 121). This reference dynamics is then compared to that of slightly heavier solid particles (density 1.4) and to air bubbles. We observe that the dynamics of the particles strongly depends on their density. Bubbles have a much faster dynamics and experience much higher accelerations than fluid tracers. Although the particles dynamics are different, we find that the probability distribution functions of accelerations normalized to the variance always remain very close to the one for the fluid tracers.

The Lagrangian approach to fluid dynamics is a natural one when one addresses problems related to mixing and transport [1]. It is widely studied in the context of intermittency in fully developed turbulence, and, in recent years, several experimental techniques have been developed in order to access Lagrangian measurements. The pioneering optical tracking method developed in the Cornell group has revealed that fluid particles experience extremely intense accelerations, with probability density functions (PDFs) having wide stretched exponential tails [2,3]. Initially limited to very short particle tracks, the technique has been extended with the use of ultrafast optical cameras [4], and is currently applied to the study of multiple particle statistics [5]. Individual particles have also been tracked for time duration of the order of the flow integral time scale using an acoustic technique [6]: in an insonified volume, individual particles scatter a sound wave whose Doppler shift carries the tracer velocity. Because of the very fast decrease of any scattering cross-section with scatterer' size, this type of method is limited to particles with size of the order of the wavelength, *i.e.* inertial ranges sizes when using acoustics [7]. However, the principle of the acoustic technique is completely analogous to laser optical Doppler velocimetry (LDV), provided that expanded light beams are used. Interference fringes are created at the intersection of two wide laser beams; a particle that crosses these fringes scatters light with a modulation frequency proportional to its velocity component perpendicular to the direction of the fringes [8]. The advantage, compared to the acoustic method, is that the much smaller wavelength allows a better resolution in space and also the use of smaller tracer particles.

In this letter, we describe the principles of this "extended" Laser Doppler technique (hereafter called "ELDV") and validate it against the known features of Lagrangian acceleration statistics in a fully turbulent von Kármán flow at $R_\lambda \leqslant 850$. We then apply it to track the dynamics of particles whose density differs from that of the fluid. The dynamics of such *inertial* particles is relevant for many engineering applications related to transport, mixing, dispersion, etc. [9]. Significant theoretical and numerical progress in this domain has

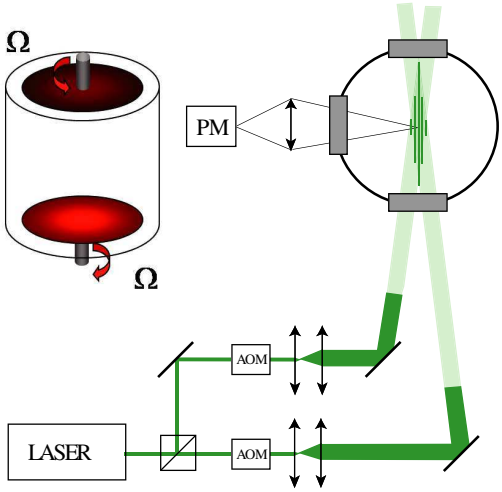

Fig. 1: Experimental setup. Left: schematics of the von Kármán flow in water —side view. Right: principle of the laser Doppler velocimetry using wide beams (ELDV) —top view of the experiment. PM: location of the photomultiplier which detects scattering light modulation as a particle crosses the interference pattern created at the intersection of the laser beams.

been made in the limiting case of infinitely heavy, pointwise particles [10] for which there is a good agreement with experimental data [11,12]. We report here the first experimental measurements of accelerations of particles having a density in the range 10^{-3} (air bubbles) to 1.4 (PMMA) in the same highly turbulent flow. Taking into account the added mass effect for small spherical particles (*i.e.* the displacement of fluid elements during the particle motion), the effective density of the bubbles is only 3 times less than that of the fluid, while the PMMA particles are roughly 1.5 times larger. Because of the mismatch of density, light particles tend to be trapped in high vortical regions: as a result of a lower inertia, the centrifugal force cannot compensate the pressure gradient which drives them into the core of the vortices [13]. On the contrary, for heavy particles the centrifugal force is stronger than the pressure gradient and they tend to be ejected from vortex cores and concentrate in high strain regions [14]. As a result of this distinct spatial sampling of the flow, particles with different buoyancies are thus expected to exhibit different dynamical behavior. We do find that the particles show different dynamical characteristics for quantities such as acceleration variance or correlation time. The PDFs of their (normalized) accelerations remain close for values less than about 10 times the acceleration variance, and differ for higher values.

Our extended laser Doppler technique is adapted from the ultrasound method developed for Lagrangian velocity measurements [6]; the gain is of a factor 1000 in wavelength so that one expects to detect micron-sized particles. Wide laser beams are used in order to follow the particle motion to get information about its dynamics in time. The optical setup is an extension of the well-known laser Doppler velocimetry technique; cf. fig. 1. A laser beam

Table 1: Parameters of the flow. Ω: rotation rate of the disks, ϵ: dissipation rate obtained from the power consumption of the motors (with an accuracy of about 20%). The Taylor-based turbulent Reynolds number is computed as $R_\lambda = \sqrt{15 u_{\rm rms}^4/\epsilon\nu}$, and a_0 is derived from the Heisenberg-Yaglom relationship —eq. (1).

Ω	$u_{\rm rms}$	$a_{\rm rms}$	τ_η	ϵ	R_λ	a_0
Hz	$\mathrm{m\cdot s^{-1}}$	$\mathrm{m\cdot s^{-2}}$	ms	$\mathrm{W\cdot kg^{-1}}$	–	–
4.1	0.5	227	0.57	4	450	4 ± 1.5
6.4	0.8	352	0.36	10	750	4.2 ± 1
8.9	1.1	826	0.24	23	850	6.4 ± 1

is split in two; each beam is then expanded with a telescope to reach a diameter of about 5 mm. They intersect in the flow and create an array of interference fringes in a volume of size of about $5 \times 5 \times 10\,\mathrm{mm}^3$. As a particle moves across the fringes, the scattered light is modulated. The frequency of modulation is directly proportional to the component of the velocity perpendicular to the interference fringes. One then measures one component of the particle velocity. In practice, we use a CW YAG laser with wavelength 532 nm at 1.2 W maximum output power. In order to get the sign of the velocity, the standard method consists in using an acousto-optic modulator (AOM) to shift the frequency of one of the beams so that the fringes are actually traveling at a constant speed. Here we use one AOM for each beam, the two excitation frequencies of the AOM being shifted by 100 kHz. The angle of the two beams is tuned to impose a 60 microns interfringe so that 100 kHz corresponds to 6 m/s. As the beams are not focused, the interfringe remains constant across the measurement volume. This volume is imaged on a photomultiplier whose output is recorded using a National Instrument PXI-NI5621 digitizer.

The flow is a turbulent von Kármán swirling flow as in the acoustics measurements [6]. Water fills a cylindrical container of internal diameter 15 cm, length 20 cm. It is driven by two disks of diameter 10 cm, fitted with blades. The rotation rate is fixed at values up to 10 Hz. For the measurements reported here, the Taylor-based Reynolds number reaches values up to 850 and the dissipation rate ϵ values up to 25 W/kg (table 1). We study three types of particles: neutrally buoyant polystyrene particles of size 31 microns and density 1.06, PMMA particles of size 43 microns and density 1.4 and air bubbles with a size of about 150 microns. The mean size of the bubbles, measured optically by imaging the measurement volume on a CCD, is imposed by the balance between the interfacial surface tension σ and the turbulent fluctuations of pressure. This fragmentation process is known to lead to a well-defined and stationary size distribution with a typical diameter $D = C\,(\sigma/\rho_f)^{3/5}\,\epsilon^{-2/5}$, ρ_f being the density of the fluid and $C \sim 0.1$ [15].

The signal processing step is crucial since both time and frequency —*i.e.* velocity— resolutions rely on its performance. Frequency demodulation is achieved using

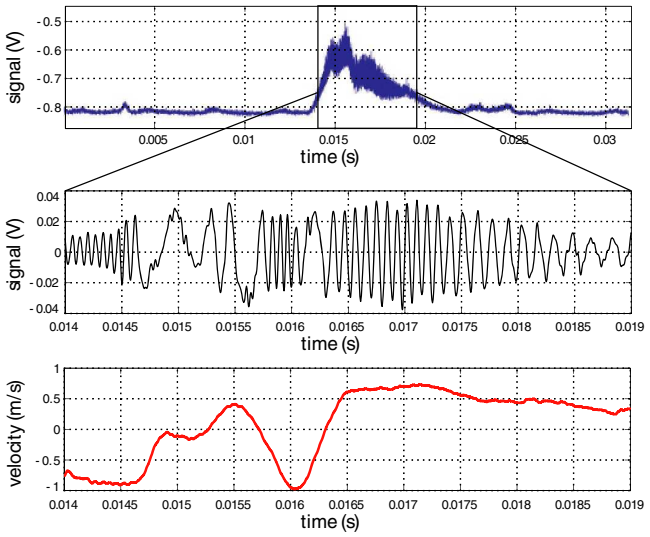

Fig. 2: Signal processing. Top: raw light modulation, as detected by the photodiode when a particle crosses the fringes. Middle: heterodyne detection of the frequency modulation. Bottom: velocity trace extracted using the approximate maximum likelihood (AML) algorithm [16].

the same algorithm as in the acoustic Doppler technique. It is an approximate maximum likelihood (AML) method coupled which a Kalman filter [16]: a parametric estimator assumes that the signal is made of a modulated complex exponential and Gaussian noise. The signal amplitude and the modulation frequencies are assumed to be slowly evolving compared to the duration of the time window used to estimate the instantaneous frequency. Here the time window is about $30\,\mu$s long and sets the time resolution of the algorithm. The outputs of the algorithm are the instantaneous frequency, the amplitude of the modulation and a confidence estimator which can be used to discriminate unreliable detections. An example of the light scattered by a particle is displayed in fig. 2, together with the Doppler frequency modulation, and final velocity signal.

Because of unavoidable noise in the measurement, we first filter out the high frequencies of the velocity signal by convolution of the velocity output with a Gaussian window of width w, and then differentiate the filtered signal to get the acceleration. The acceleration variance is computed using the same procedure as in [3]: it is obtained for several widths of the smoothing kernel used in the differentiation of the velocity signal and then interpolated to zero filter width (fig. 3(a)). As shown in fig. 3(b), since measurements are performed only when a particle moves within the (limited) measurement volume, the data consists in a collection of sequences with variable durations. We have checked that the acceleration variance weakly depends on the duration of the trajectories used for the computation (inset of fig. 3(b)), thus leading to an unbiased estimation of $a_{\rm rms}$.

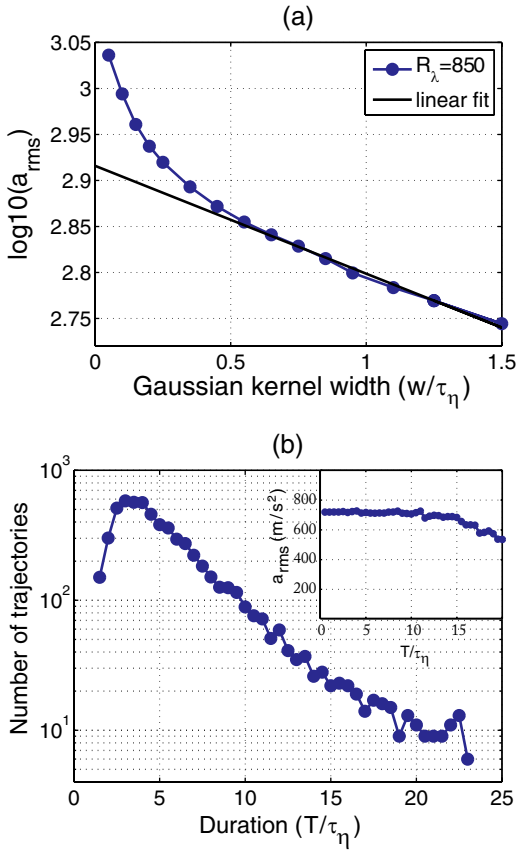

Fig. 3: (a) Evolution of the acceleration variance logarithm with the smoothing kernel width w/τ_η for neutral particles at $R_\lambda = 850$. (b) Number of trajectories of duration T for the same data set (7000 trajectories corresponding to 10^7 data points). The inset shows the evolution of the acceleration variance with T when only trajectories longer than T are used for the computation.

We first compare our data for neutral particles to the Cornell measurement using high-speed imaging [2,3]: their data was obtained using linear cameras with 512 pixels running at speeds up to 70000 frames per seconds. The probability density functions (PDFs) of the acceleration, from our ELDV technique at increasing Reynolds numbers and for the Cornell data at $R_\lambda = 690$ are shown in fig. 4: the distributions are in very good agreement both qualitatively and quantitatively. Note that in order to compare the two experiments, the Heisenberg-Yaglom scaling is used for the normalization of the acceleration variance

$$\langle a^2 \rangle = a_0 \epsilon^{3/2} \nu^{-1/2}, \qquad (1)$$

where ϵ is the dissipation rate per unit mass and $\nu = 1.3 \cdot 10^{-6}\,\mathrm{m}^2 \cdot \mathrm{s}^{-1}$ is the kinematic viscosity of water. We measure $a_0 = 6.4 \pm 1$ at $R_\lambda = 850$ compared to 6.2 ± 0.4 for the Cornell data at $R_\lambda = 690$, both acceleration variances being computed using the same procedure [3]. The acceleration autocorrelation function, shown in fig. 4b, decays in a time of the order of the Kolmogorov time $\tau_\eta = \sqrt{\nu/\epsilon}$, the fastest time scale of the turbulent flow.

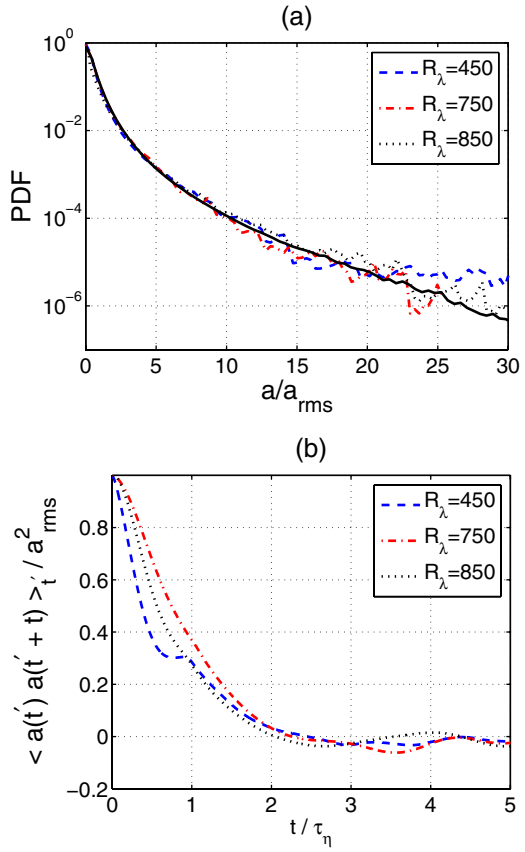

Fig. 4: (a) Probability density functions (PDFs) of the acceleration, normalized by its variance, for neutral particles. Dashed, dotted, dash-dotted lines: ELDV measurements; black solid line: Cornell data at $R_\lambda = 690$. (b) Autocorrelation coefficients of the accelerations for the same cases.

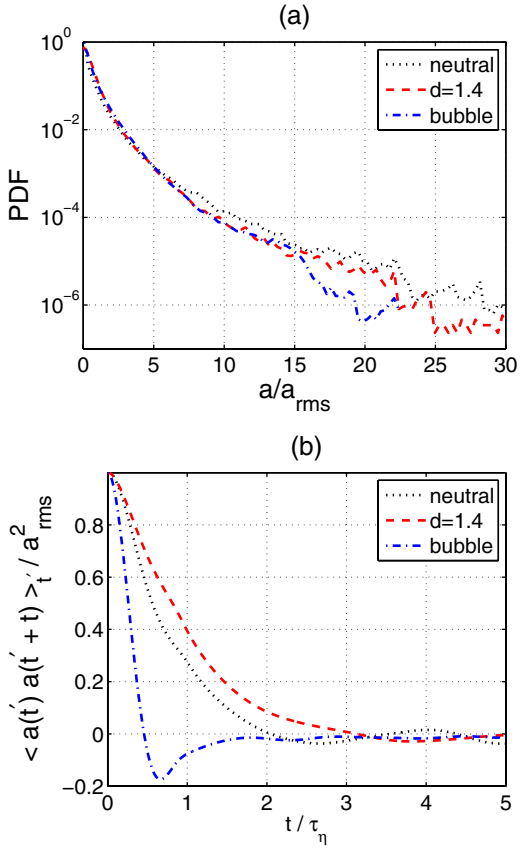

Fig. 5: (a) Probability distribution function of accelerations, normalized to the variance of the data sets. Flow at $R_\lambda = 850$. (b) Normalized autocorrelation coefficient of the acceleration.

These results confirms that our techniques achieves a fast enough time and velocity resolution to get a good estimate of particle acceleration. As they have lower velocities and accelerations at low Reynolds number, it is more difficult to separate the particles acceleration at $R_\lambda = 450$ from the short correlation noise. As previously shown in [2] using the same type of filtering, this is at the origin of the slight difference at small times for the correlation curve at $R_\lambda = 450$ compared to the other cases.

We now apply our technique to compare Lagrangian tracers to the dynamics of heavier and lighter particles. We first compute the velocity root mean square value $u_{\rm rms}$ for all three cases: the values are $1.1, 1.2, 1.0 \pm 0.1\,{\rm m\cdot s^{-1}}$ at $R_\lambda = 850$ for the neutral, heavy (PMMA spheres) and light particles (bubbles). These values are identical within error bars. It indicates that the large-scale dynamics of the particles is unaffected by changes in their density (inertia). The acceleration distribution and autocorrelation are shown in fig. 5. When normalized by the acceleration variance, the acceleration PDFs are quite similar for acceleration values below about $15 a_{\rm rms}$, as also observed in low Reynolds number numerical simulations [17]. The normalized acceleration variance a_0 varies very significantly as shown in table 2: it is reduced to 4.3 ± 1 for heavier particles at $R_\lambda = 850$ while it is increased to 26 ± 5 for bubbles. Note that in dimensional units, the rms acceleration for bubbles is $159\,g$ so that accelerations events a of $15\,a_{\rm rms}$ amplitude (not uncommon as shown in the PDF) corresponds to almost $2400\,g$. The correlation functions also display significant changes with the inertia: the characteristic time of decay is longer for heavy particles and much shorter for bubbles compared to neutral particles. We obtain $\tau_{\rm corr}/\tau_\eta = 0.5, 0.9, 0.25$ respectively, for neutral, heavy and light particles, with the correlation time defined as the half-width at mid-amplitude of the

Table 2: Parameters of the particles at $R_\lambda = 850$ ($\eta = (\nu^3/\epsilon)^{1/4} = 17\,\mu$m and $\tau_\eta = \sqrt{\nu/\epsilon} = 0.26\ 10^{-3}$ s). ρ_p and ρ_f are the densities of the particles and fluid, and $\tau_{\rm corr}$ is defined as the half-width at mid amplitude of the acceleration autocorrelation function.

Particles	radius a	$\beta = \dfrac{3\rho_f}{\rho_f + 2\rho_p}$	$\dfrac{\tau_{\rm corr}}{\tau_\eta}$	a_0
Tracers	$15.5\,\mu$m	0.96	0.5	6.4 ± 1
Heavy	$20.5\,\mu$m	0.79	0.9	4.3 ± 1
Bubbles	$75\,\mu$m	2.99	0.25	26 ± 5

correlation function. We thus observe significant changes in the dynamics, even if the (normalized) distributions of accelerations change weakly with inertia.

We now briefly discuss these results. In order to characterize the dynamics of a solid particle, one must specify two dimensionless numbers: the Stokes number which, in the case of turbulent flows, is the ratio of the response time of the particle to the Kolmogorov time scale, and the density ratio of the particle to that of the fluid. In the asymptotic case of large inertia, only the Stokes number matters [10]. However, in the measurements reported here inertia remains finite, even for the bubble case because of added mass effects. In the limit of small particle sizes compared to the Kolmogorov length scale one generally uses the equation of motion for a solid particle [18,19]:

$$\frac{\mathrm{d}\mathbf{v}_p}{\mathrm{d}t} = \beta \frac{D\mathbf{u}}{Dt} + \mathbf{F}, \tag{2}$$

where $\mathbf{v}_p$ is the particle velocity, $\beta = 3\rho_f/(2\rho_p + \rho_f)$, ρ_f and ρ_p are the fluid and particle specific mass, respectively), $D\mathbf{u}/Dt$ is the acceleration of the fluid particle that would be at the position of the solid particle in the undisturbed flow and $\mathbf{F}$ incorporates other forces such as drag, lift, history and possibly buoyancy. Here, $\beta = 1$, 0.8 and 3 for our neutral, heavy and light particles. Note that bubbles with such a small diameter are usually considered as being rigid because of impurities in the fluid [20], with a boundary condition which may be different from that of a solid particle. Qualitatively, we find that the trend for the measured acceleration variance follows that of β in eq. (2). Quantitatively, for heavy particles it changes roughly as β, but for the bubbles, which may be not considered as pointwise since their radius is $a \sim 5\eta$, the acceleration variance is only about 2 times that of the fluid. This is different from what was reported in [2] where a stronger influence of small change in the particles density was observed.

To conclude, we have reported here an extended laser Doppler velocimetry technique (ELDV) for the tracking of individual particles in fully developed turbulence. Its advantage is that it may be more easily adapted from commercial equipment than ultrafast PIV, and requires less laser power for illumination. The very close agreement between the measurements reported here and the Cornell [3] data is expected because they share the same flow geometry. The fact that it is observed using two very different techniques and signal processing validates both (as the performance of the high-speed imaging method had not been matched previously). Application of the ELDV technique to the study of inertial particles with a finite density shows that quite different dynamics may lead to very similar statistics of (normalized) particle accelerations, an observation that may prove useful for modeling.

* * *

We are indebted to A. Petrosian for his help in setting up the optics of the experiment, and to M. Bourgoin for many fruitful discussions. This work was partially funded by the Region Rhône-Alpes, under Emergence Contract No. 0501551301.

REFERENCES

[1] Fox R. O. and Yeung P. K., *Phys. Fluids*, **15** (2003) 961; Sawford B., *Annu. Rev. Fluid Mech.*, **33** (2001) 289.
[2] Voth G. A., La Porta A., Crawford A. M., Alexander J. and Bodenschatz E., *J. Fluid Mech.*, **469** (2002) 121.
[3] Mordant N., Crawford A. M. and Bodenschatz E., *Physica D*, **193** (2004) 245; *Phys. Rev. Lett.*, **94** (2004) 024501.
[4] Xu H. *et al.*, *Phys. Rev. Lett.*, **96** (2006) 024503.
[5] Lüthi B., Ott S., Berg J. and Mann J., *Phys. Rev. E*, **74** (2006) 016304; Bourgoin M. *et al.*, *Science*, **311** (2006) 835; Xu H., Ouellette N. T., Nobach H. and Bodenschatz E., *ETC11 Proceedings* (Springer) 2007.
[6] Mordant N. *et al.*, *Phys. Rev. Lett.*, **87** (2001) 214501; Mordant N., Metz P., Michel O. and Pinton J.-F., *Rev. Sci. Instrum.*, **76** (2005) 025105.
[7] Mordant N., Lévêque E. and Pinton J.-F., *New J. Phys.*, **6** (2004) 116.
[8] Lehmann B., Nobach H. and Tropea C., *Meas. Sci. Technol.*, **13** (2002) 1367.
[9] Falkovich G., Fouxon A. and Stepanov M., *Nature*, **419** (2002) 151; Shaw R., *Annu. Rev. Fluid Mech.*, **35** (2003) 183.
[10] Bec J., Cencini M. and Hillerbrand R., *Physica D*, **226** (2007) 11; Bec J. *et al.*, *Phys. Rev. Lett.*, **98** (2007) 084502.
[11] Fessler J. R., Kulick J. D. and Eaton J. K., *Phys. Fluids*, **6** (1994) 3742.
[12] Ayyalasomayajula S., Gylfason A., Collins L. R., Bodenschatz E. and Warhaft Z., *Phys. Rev. Lett.*, **97** (2006).
[13] Calzavarini E., Cencini M., Lohse D. and Toschi F., *Advances in Turbulence XI* (Springer) 2007, ISBN: 978-3-540-72603-6, pp. 418–420.
[14] Sundaram S. and Collins L. R., *J. Fluid Mech.*, **379** (1999) 105.
[15] Martinez-Bazá C., Montañés J.-L. and Lasheras J. C., *J. Fluid Mech.*, **401** (1999) 183.
[16] Mordant N., Michel O. and Pinton J.-F., *J. Acoust. Soc. Am.*, **112** (2002) 108.
[17] Mazzitelli I. M. and Lohse D., *New J. Phys.*, **6** (2004) 203.
[18] Maxey M. R. and Riley J., *Phys. Fluids*, **26** (1983) 883.
[19] Howe M. S., *Q. J. Mech. Appl. Math.*, **48** (1995) 401.
[20] Duineveld P. C., *J. Fluid Mech.*, **292** (1995) 325.